19th Australasian Fluid Mechanics Conference
Melbourne, Australia
8-11 December 2014

Global and Convective Stability of Horizontal Convection

T. K. Tsai[1], **W. K. Hussam**[1] **and G. J. Sheard**[1]

[1]The Sheard Lab, Department of Mechanical and Aerospace Engineering
Monash University, Melbourne, Victoria 3800, Australia

Abstract

The current study seeks to identify the mechanism responsible for the instability leading to unsteady flow in horizontal convective flow. A one-dimensional (1D) linear stability analysis algorithm is developed which linearises the momentum and energy equations under the Boussinesq approximation, and is applied to vertical velocity and temperature profiles extracted from computed two-dimensional flow solutions. It is demonstrated that a Rayleigh–Bénard type transverse roll instability within the thermal layer ultimately leads to formation of plumes and consequently gives rise to unsteady flow in horizontal convection.

Introduction

Temperature gradients within a fluid give rise to density differences that produce buoyancy driven flows. Horizontal convection (HC) describes the motion of fluid due to uneven heating along one horizontal boundary [17] [1]. The key parameter characterizing horizontal convection is Rayleigh number, which quantifies the strength of thermal forcing on the flow.

Instability and mixing are known to be very important in geophysical flow [8]. Many theoretical oceanographers [3, 21, 6] argued that HC alone is insufficient to drive a significant overturning geophysical flow. Paparella *et al.*[10] illustrated that HC alone does not statisfy the "zeroth" law to be a true trubulent flow. This true turbulent test for HC has been disputed by Scotti *et al.*[13] as being too restrictive, rendering Rayleigh–Bénard convection non-turbulent as well, and that statistically HC has the characteristic of a turbulent flow. The unsteadiness of HC was investigated numerically [16, 2, 4] and experimentally [20, 5] to show that HC is unsteady and turbulent at high Rayleigh number, able to propagate through the entire domain to create an overturning circulation. However, the flow transition mechanism is still an open question. As noted by Hughes *et al.*[5], horizontal convection takes place without an instability, the terms stabilizing/destabilizing buoyancy were used to describe instability in HC flow.

The onset of convective instability in Rayleigh–Bénard convection (RBC) and Rayleigh–Bénard–Poiseuille (RBP) flows have been studied extensively. In RBC, instability invokes convection beyond a critical Rayleigh number as buoyancy of the heated bottom layer of fluid overcomes the stabilising viscous damping and manifests as transverse convective rolls. In constrast, the through-flow in RBP acts as a selection mechanism determining the direction of the convective instability roll. However, it was found that Rayleigh–Bénard type instability is unaffected by low velocity through-flow. This is similar to the forcing boundary layer in horizontal convection, where the overturning flow velocities are low at Rayleigh number where the flow remains steady ($Ra \leq 5\times10^8$). Sun [18] subsequently looked into the instability mechanism of HC flows. His numerical experiment involved thermal forcing at the centre as well as side-wall forcing with two circulating cells. He concluded that velocity shear instability rather than thermal instability is responsible for the unsteady HC flow through a Hopf bifurcation with a critical Rayleigh number of 5.5377×10^8 at $Pr=1$. In contrast to [18], the present work considers HC with one circulating cell at $Pr=6.14$, such as those investigated by Gayen *et al.*[4].

A local stability analysis is used here to explain the instability mechanism of HC flows. In constrast to the view conveyed in [4] that unsteady flow originate in the plume, instead we turn our attention to the forcing boundary layer. The aim of the present work is to elucidate the mechanism of horizontal convection instability through local one-dimensional (1D) linear stability analysis.

Numerical Setup

The system comprises a rectangular enclosure of width L and height H. The flow is driven by a non-uniform constant temperature profile applied along the bottom of the enclosure.

The side and top walls are insulated (a zero temperature gradient is imposed normal to the wall), and a no-slip condition is imposed on the velocity field on all walls. A Boussinesq approximation for fluid buoyancy is employed, in which density differences in the fluid are neglected except through the gravity term in the momentum equation. Under this approximation the energy equation reduces to a scalar advection-diffusion equation for temperature which is evolved in conjunction with the velocity field. The fluid temperature is related linearly to the density via the thermal expansion coefficient α. The dimensionless Navier–Stokes equations governing a Boussinesq fluid may be written as

$$\frac{\partial \mathbf{u}}{\partial t} = -(\mathbf{u}\cdot\nabla)\mathbf{u} - \nabla p + Pr\nabla^2\mathbf{u} - PrRa\hat{\mathbf{g}}T, \tag{1}$$

$$\nabla\cdot\mathbf{u} = 0, \tag{2}$$

$$\frac{\partial T}{\partial t} = -(\mathbf{u}\cdot\nabla)T + \nabla^2 T, \tag{3}$$

where $\mathbf{u}$, p, t, Ra, Pr, $\hat{\mathbf{g}}$ and T are the velocity vector, kinematic static pressure, time, Rayleigh number, Prandtl number, a unit vector in the direction of gravity, and temperature, respectively. Lengths are scaled by the enclosure width L, velocities by κ_T/L (where κ_T is the thermal diffusivity of the fluid), time by L^2/κ_T, and temperature by δT (the imposed temperature difference imposed across the bottom wall). The horizontal Rayleigh number is defined as $Ra = g\alpha\delta T L^3/\nu\kappa_T$, where g is the gravitational acceleration and ν is the kinematic viscosity of the fluid. The Prandtl number of the fluid is given as $Pr=\nu/\kappa_T$, and throughout this study $Pr=6.14$, which approximates water at laboratory conditions. The Nusselt number, a measure of the ratio of convective to conductive heat transfer, is defined as $Nu = F_T L/\rho c_p \kappa_T \delta T$. The heat flux is given by $F_T = \kappa_T \rho c_p(\overline{\partial T/\partial y})$, where c_p is the specific heat capacity of

[1]Rayleigh–Bénard convection (RBC) occurs under the influence of a temperature gradient across two opposing boundaries. Rayleigh–Bénard–Poiseuille describes a RBC with a through flow.

the fluid, and $\overline{\partial T/\partial y}$ is the average absolute vertical temperature gradient along the forcing boundary.

Two-dimensional solutions are computed using a high-order spectral element method for spatial discretization and a third-order time integration scheme based on backward-differencing. This code had been validated in a number of studies on wake dynamics of flow over bluff bodies [14] [15].

1D Linear Stability Analysis

We are interested in the stability of one-dimensional base flows ($\mathbf{u}_B$, p_B, θ_B) extracted from two-dimensional solutions along lines of constant x (*i.e.* $\partial/\partial x \ll \partial/\partial y$ and $\partial/\partial z \ll \partial/\partial y$) to small three-dimensional time-dependent perturbation of velocity (u,v,w), pressure p or temperature, θ of the form

$$f = f_B + \delta \tilde{f} e^{(\mathrm{i}(\alpha x + \beta z - \omega t))}, \tag{4}$$

where δ is an arbitrary small constant. The perturbation comprises a travelling wave number component (α,β) in x and z directions, and a frequency and growth rate dictated by ω. The disturbance equations are obtained by substituting equation (4) into (1)-(3), subtracting the base flow equations, and neglecting $O(\delta^2)$ terms. The exponential terms subsequently cancel, and following the similar approach to the derivation of the Orr–Sommerfeld equation [11, 12], the continuity and momentum equations are combined to eliminate $\tilde{u}$, $\tilde{w}$ and $\tilde{p}$. The problem then reduces to

$$\begin{aligned} \mathrm{i}\alpha\left[u_B'' - u_B(\mathrm{D}^2 - k^2)\right]\tilde{v} + Pr(\mathrm{D}^2 - k^2)^2\tilde{v} \\ -PrRak^2\tilde{\theta} = \mathrm{i}\omega(\mathrm{D}^2 - k^2)\tilde{v}, \end{aligned} \tag{5}$$

$$\theta_B'\tilde{v} + u_B\mathrm{i}\alpha\tilde{\theta} - (\mathrm{D}^2 - k^2)\tilde{\theta} = \mathrm{i}\omega\tilde{\theta}, \tag{6}$$

where the operator D evaluates partial derivatives with respect to y, $k^2 = \alpha^2 + \beta^2$, and primes denote differentiation with respect to y. As per convention, we seek solutions subject to the boundary conditions

$$\tilde{v}(0) = \tilde{v}(H) = \frac{\mathrm{d}\tilde{v}(0)}{\mathrm{d}y} = \frac{\mathrm{d}\tilde{v}(H)}{\mathrm{d}y}, \frac{\mathrm{d}\tilde{\theta}(0)}{\mathrm{d}y} = \frac{\mathrm{d}\tilde{\theta}(H)}{\mathrm{d}y} = 0. \tag{7}$$

Equations (5)-(7) are discretised using a Chebychev collocation method [19], and are of the form $A\mathrm{x}_k = \omega_k B\mathrm{x}_k$. Eigenvector x_k is a concatenation of the vectors of collocation-point values of $\tilde{v}$ and $\tilde{\theta}$, i.e. $\mathrm{x}_k = [\tilde{v}\ \tilde{\theta}]^T$. The k-th eigenvalue $\omega = \omega_r + \mathrm{i}\omega_i$ describes spatio-temporal mode evolution through $e^{\omega_i t}(\cos\omega_r t - i\sin\omega_r t)$. The imaginary part provides the growth rate, with instability corresponding to $\omega_i > 0$, while the real part gives the angular frequency of any oscillatory component of the instability mode. Transverse roll instability is investigated by keeping β fixed and finding α maximising $\mathrm{Im}(\omega)$. Longitudinal roll instability is investigated by keeping α fixed and finding β maximising $\mathrm{Im}(\omega)$.

The stability code was validated against an accurate numerical result [9], where the critical Reynolds number of $Re_c = 5772.22$ and wavenumber $\alpha_c = 1.02056$ for plane Poiseuille flow were reproduced.

Result and Discussion

A numerical experiment on a rectangular enclosure with an imposed linear temperature profile at the bottom boundary with insulated top and side walls was conducted with an aspect ratio of $H/L = 0.16$. With the imposed linear temperature profile on the bottom wall, heat is being extracted at the cold end while the fluid at the hot end is being heated. With higher temperature at

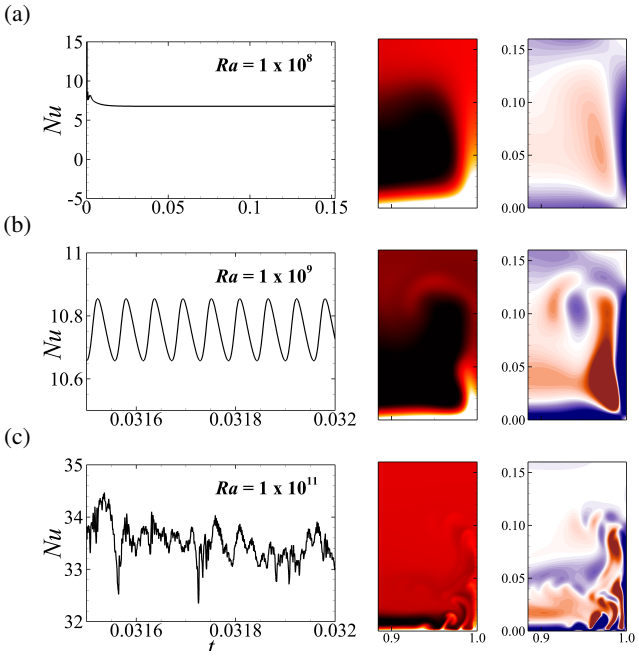

Figure 1. A plot of Nusselft number against time with the corresponding temperature and vorticity contour at the hot corner of the enclosure with different Rayleigh number as stated. Dark to light temperature contours show temperatures ranging from $0.225 \leq T \leq 0.375$. The minimum and maximum levels of the vorticity contours for $Ra = 10^8, 10^9$ and 10^{11}, respectively are 1×10^{-5} to 1×10^5, 1×10^{-5} to 1×10^5 and 2×10^{-6} to 2×10^6

the hot end, fluid is carried upward with buoyancy forcing due to the density stratification in the heated region. The fluid from the cold end will move toward the heated end to fill the void left by the heated buoyant fluid which rises upward. The warm fluid will move upward and gradually fall back down toward the cold end and thus complete an overturning circulating cell within the enclosure. The characteristics and strength of this circulation are determined by the Rayleigh number.

At low Rayleigh number, where the imposed temperature is mainly transmitted through conduction into the enclosure, the flow will reach a time steady solution where distinct boundary layer is observed along the forcing boundary. With further increases in Rayleigh number, the flow enters a mixed conduction/convection regime, and remains time invariant. Beyond $Ra \approx 3.2\times10^8$, a convection-dominant flow appears leading to a time-periodic solution. With a further increase in Rayleigh number, time periodicity is broken, giving way to an irregular regime. The nature of these regimes is demonstrated in figure 1 where the Nusselt number time history and instantaneous flow fields are plotted. A time periodic solution is clearly seen at $Ra = 1\times10^9$; at this Rayleigh number disturbances are advected along the thermal boundary layer and feeding into the rising plume. As the plume rises to mid-height, all internal energy has been converted to potential and kinectic energy. Subsequently, the plume descends and creates a small local circulation zone near the corner of the hot wall. This plume lack the energy to rise up to the top to create a larger circulation as seen in cases with higher Rayleigh number. With higher Rayleigh number, figure 1(c) shows a low frequency oscillation superimposed on the time periodic flow, this can be seen at $Ra \geq 3.2\times10^9$. At these Rayleigh numbers, the plume has sufficient energy to rise beyond the mid height, with some partial plume break-up observed at mid height to form a local circulation and the majority of it rises to the top, mixed with the bulk flow to form a

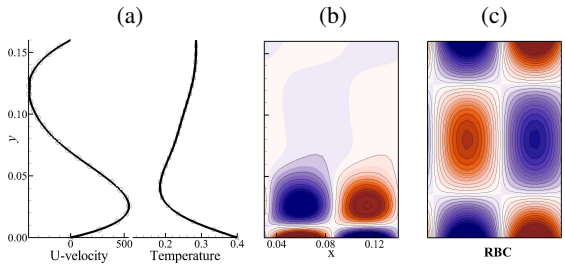

Figure 2. (a) A plot of local dimensionless horizontal velocity and temperature profile at $x = 0.9$ for $Ra = 1 \times 10^8$. (b) A contour plot of the perturbation vorticity at x=0.90 from the 1D stability analysis showing the instability is confined to a boundary layer region along the lower boundary. (c) A contour plot of perturbation vorticity for RBC is included for comparison.

much larger overturning circulation over the whole enclosure. It is this large global circulation which superimposes the low frequency oscillation over the higher frequency plume formation. The interaction of this global and local circulation creates a more irregular flow characteristic within the enclosure which breaks the periodicity of the flow. This large scale global and local transport interaction was discussed in a recent review by Ahlers *et al.*[1].

To initiate our 1D LSA, local profiles at different x-locations were used as base flow condition to solve for the linear stability eigenmodes. Figure 2 (a) shows extracted u & θ profiles at $x = 0.90$ for $Ra = 1 \times 10^8$. The wavenumber producing the maximum growth is $\alpha = 58$, figure 2 (b) plots the perturbation vorticity field of the corresponding eigenvector field. By comparison, figure 2 (c) shows the vorticity field for RBC instability. The leading perturbation shows that instability indeed is confined to a thin boundary layer adjacent to the bottom surface, corresponding to the region of the flow with a strong adverse temperature gradient, consistent with the canonical RBC flow. The vorticity exhibits a counter-rotating structure which resembles RBC instability. In this region the velocity profiles do not exhibit any inflexion, which is neccessing but not sufficient for shear instability according to Rayleigh inflexion point theorem [7]. These results combined to show that HC instability is thermally driven rather than a velocity shear instability in contrast to [18].

The conjecture that HC instability is a thermal instability due to an RBC instability mechanism is tested by independently performing the analysis on the velocity and temperature base flow profiles separately. Isolated local velocity or temperature profiles are used to study instability for $Ra = 1 \times 10^8$. Figure 3 shows the differences in growth rate when only the velocity or temperature profile is used. The thermal profile produces almost identical growth up to wavenumbers exceeding the dominant wavenumber; whereas the velocity profile remains stable and monotonically decreases with increasing α. At the dominant wavenumber, the eigenmode produced by the thermal profile is almost indistinguishable from the reference case, whereas the velocity profile produces a completely different disturbance structure. This confirms that the instability is thermally driven, and is virtually insensitive to the velocity profiles.

Figure 4 maps marginal stability curves for different locations along the forcing boundary, showing larger unstable regions towards the heated end of the enclosure. Local instability was found to progressively advance upstream with increasing Rayleigh number. As the location of local instabilities moves upstream, more energy is accumulated as disturbances advect

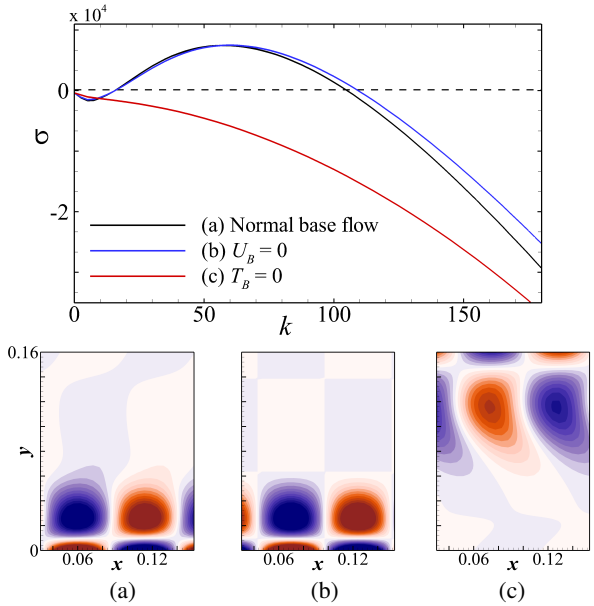

Figure 3. A plot of wavenumber, k, against growth rate, σ at $x = 0.90$ for $Ra = 1 \times 10^8$, positive growths were found when (a) local base flow profiles were used and when (b) local base flow velocity was set to zero. Negative growth rate was obtained when (c) base flow temperature was set to zero. Respective perturbation vorticity contours are included for comparison.

in the forcing boundary layer, eventually leading to global instability. For instance, at $Ra = 3.2 \times 10^9$, local instability was found from $x = 0.70$ onward, which generates sufficient amplification to tip the flow to global instability. The marginal Rayleigh number can be extrapolated to $x = 1$, yielding a critical marginal Rayleigh number of $Ra_{\mathrm{cm}} = 1.23 \times 10^7$.

In order to verify the 1D stability analysis and to elucidate on the mechanism of HC instability, a two-dimensional perturbation analysis was performed on a time steady solution with $Ra = 1 \times 10^8$. This steady solution is seeded with random perturbation before continuing with time integration. Random features quickly dissipated, isolating the dominant disturbance in the flow (figure 5) The disturbance in figure 5 is consistent in structure to that predicted in figure 2(b), and has a similar wavelength ($\lambda_{2\mathrm{D}} = 0.07452$) to that predicted by the 1D analysis ($\lambda_{1\mathrm{D}} = 0.1073$).

Conclusion

We have shown that a one-dimensional linear stability analysis can elucidate the instability mechanism in horizontal convection, revealing it to be themally driven and consistent with Rayleigh–Bénard convection instability.

Acknowledgement

This work is supported by ARC Discovery Grant DP120100153, and a high-performance computing time allocation through the National Computational Infrastructure (NCI) Merit Allocation Scheme and Monash SunGrid system through Monash e-Research Centre.

References

[1] Ahlers, G., Grossmann, S. & Lohse, D., Heat transfer and large scale dynamics in turbulent Rayleigh–Bénard convection, *Reviews of modern physics* **81** (2), 2009, 503.

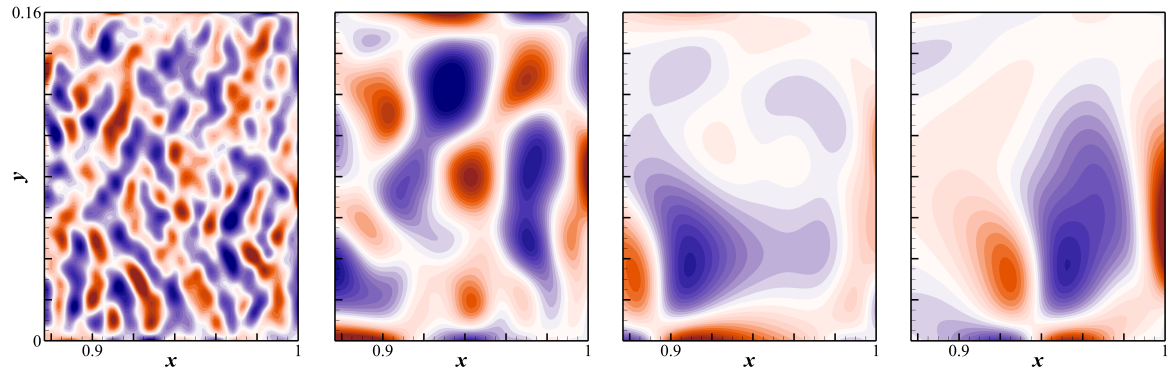

(a) $t = 0$ (b) $t = 10$ (c) $t = 50$ (d) $t = 80$

Figure 5. A contour plot of the perturbation vorticity from 2D perturbation simulation at various computed time step with a step size of 7×10^{-9}. (a) shows the initial random perturbation seeded in the domain, (b)-(d) show time evolution of the perturbation vorticy.

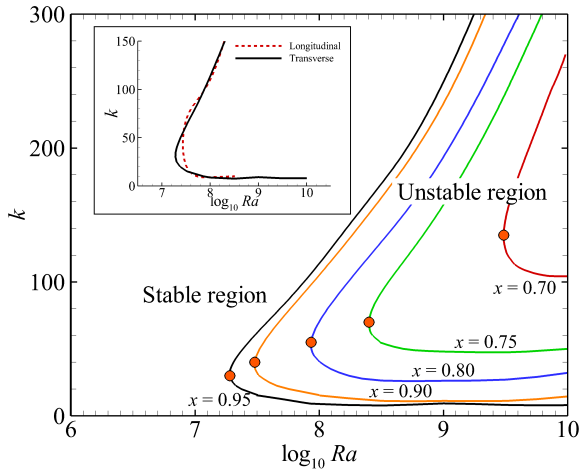

Figure 4. Marginal stability plot of $log_{10}Ra$ against wavenumber, k, at various x-locations. Each curve mapped out stable and unstable range of Ra for that specific location with marginal Ra indicated by a circle mark. An inset showing a marginal stability curve for perturbation in the longitudinal and transverse directions, at $x = 0.95$.

[2] Coman, M., Griffiths, R. & Hughes, G., The sensitivity of convection from a horizontal boundary to the distribution of heating, *Journal of Fluid Mechanics* **647**, 2010, 71.

[3] Defant, A., *Physical oceanography; volume 1*, 1961, Pergamon Press.

[4] Gayen, B., Hughes, G. O. & Griffiths, R. W., Completing the mechanical energy pathways in turbulent Rayleigh–Bénard convection, *Physical review letters* **111** (12), 2013, 124301.

[5] Hughes, G. & Griffiths, R., Horizontal convection, *Annu. Rev. Fluid Mech.* **40**, 2008, 185–208.

[6] Kuhlbrodt, T., Griesel, A., Montoya, M., Levermann, A., Hofmann, M. & Rahmstorf, S., On the driving processes of the atlantic meridional overturning circulation, *Reviews of Geophysics* **45** (2), 2007.

[7] Lin, C., On the stability of two-dimensional parallel flows, *Proceedings of the National Academy of Sciences of the United States of America* **30** (10), 1944, 316.

[8] McWilliams, J. C., The emergence of isolated coherent vortices in turbulent flow, *Journal of Fluid Mechanics* **146**, 1984, 21–43.

[9] Orszag, S. A., Accurate solution of the Orr–Sommerfeld stability equation, *J. Fluid Mech* **50** (4), 1971, 689–703.

[10] Paparella, F. & Young, W., Horizontal convection is non-turbulent, *Journal of Fluid Mechanics* **466**, 2002, 205–214.

[11] Reddy, S. C., Schmid, P. J. & Henningson, D. S., Pseudospectra of the Orr–Sommerfeld operator, *SIAM Journal on Applied Mathematics* **53** (1), 1993, 15–47.

[12] Schmid, P. J. & Henningson, D. S., *Stability and Transition in Shear Flows*, New York: Springer, 2001.

[13] Scotti, A. & White, B., Is horizontal convection really non-turbulent?, *Geophysical Research Letters* **38** (21), 2011.

[14] Sheard, G. J., Leweke, T., Thompson, M. C. & Hourigan, K., Flow around an impulsively arrested circular cylinder, *Physics of Fluids* **19**, 2007, 083601.

[15] Sheard, G. & Ryan, K., Pressure-driven flow past spheres moving in a circular tube, *Journal of Fluid Mechanics* **592**, 2007, 233–262.

[16] Siggers, J., Kerswell, R. & Balmforth, N., Bounds on horizontal convection, *Journal of Fluid Mechanics* **517** (1), 2004, 55–70.

[17] Stern, M. E., *Ocean circulation physics*, vol. 246, Academic Press New York, 1975

[18] Sun, L., MA, D.-J., Zhang, W. & Sun, D.-J., Onset of unsteady horizontal convection in rectangle tank at $Pr = 1$, *arXiv preprint physics/0702037*, 2007.

[19] Trefethen, L. N., *Spectral methods in MATLAB*, vol, 10, Siam, 2000.

[20] Wang, W. & Huang, R. X., An experimental study on thermal circulation driven by horizontal differential heating, *Journal of Fluid Mechanics* **540** (1), 2005, 49–73.

[21] Wunsch, C. & Ferrari, R., Vertical mixing, energy, and the general circulation of the oceans, *Annu. Rev. Fluid Mech.* **36**, 2004, 281–314.